SURAT TUGAS
Nomor: 195-R/UNTAR/PENELITIAN/IV/2024

Rektor Universitas Tarumanagara, dengan ini menugaskan kepada saudara:

ANDY PRABOWO PHO, S.T., M.T., Ph.D.

Untuk melaksanakan kegiatan penelitian/publikasi ilmiah dengan data sebagai berikut:

Judul	:	Stability design of cold-formed high and ultra-high strength steel thin-walled box sections using effective stress-strain model
Nama Media	:	Structures
Penerbit	:	Elsevier
Volume/Tahun	:	62/106189/2024
URL Repository	:	https://www.sciencedirect.com/science/article/abs/pii/S2352012424003412

Demikian Surat Tugas ini dibuat, untuk dilaksanakan dengan sebaik-baiknya dan melaporkan hasil penugasan tersebut kepada Rektor Universitas Tarumanagara

01 April 2024
Rektor

UNIVERSITAS TARUMANAGARA
REKTOR

Prof. Dr. Ir. AGUSTINUS PURNA IRAWAN

Print Security : 11185a9d3232cb3a0c745895f4735ce6

Disclaimer: Surat ini dicetak dari Sistem Layanan Informasi Terpadu Universitas Tarumanagara dan dinyatakan sah secara hukum.

The Institution of
StructuralEngineers

ELSEVIER

Structures

Research Journal of The Institution of Structural Engineers

ScienceDirect

Structures

4.7
CiteScore

4.1
Impact Factor

Submit your article

Guide for authors

Menu

Search in this journal

- Aims and scope
- **Editorial board**
- Call for papers
- News
- Conferences
- Featured Articles
- Impact Statements

Editorial board by country/region

57 editors and editorial board members in 15 countries/regions

1 United Kingdom (18)
2 China (10)
3 United States of America (6)

> See more editors by country/region

Editorial board

Editor-in-Chief

Leroy Gardner, PhD

Imperial College London, London, United Kingdom

View full biography

Associate Editors

Ashraf Ashour, PhD, FIStructE

University of Bradford, Bradford, United Kingdom

Muhammed Basheer, PhD, DSc

University of Leeds, Leeds, United Kingdom

Mark A. Bradford, PhD DSc

University of New South Wales, Sydney, Australia

Yao Chen, PhD, Professor

Southeast University, Nanjing, China

Mario D'Aniello, PhD

University of Naples Federico II, Napoli, Italy

Hosssein Derakhshan, PhD

Queensland University of Technology, Brisbane, Queensland, Australia

Mohamed Elchalakani, PhD

The University of Western Australia, Department of Civil Environmental and Mining Engineering, Perth, Australia

Ana Espinós, PhD

Polytechnic University of Valencia, Valencia, Spain

All members of the Editorial Board have identified their affiliated institutions or organizations, along with the corresponding country or geographic region. Elsevier remains neutral with regard to any jurisdictional claims.

ELSEVIER

RELX™

Volume 62

In progress (April 2024)

This issue is in progress but contains articles that are final and fully citable.

Structures

Research article ○ Abstract only

Research on the axial compressive behavior of double skin composite wall with steel truss

Ke-Rong Luo, Gan-Ping Shu, Zhong-Hua Liu
Article 106159

Article preview

Research article ○ Abstract only

Performance evaluation of innovative triangular and spherical ribbed headed studs in composite steel beam-concrete slab junction

Prakash Abhiram Singh, Yogesh Deoram Patil, Rahul Tarachand Pardeshi
Article 106137

Article preview

Research article ○ Abstract only

Computational design of segmented concrete shells made of post-tensioned precast flat tiles

Francesco Laccone, Sandro Menicagli, Paolo Cignoni, Luigi Malomo
Article 106156

Article preview

Research article ○ Abstract only

Robustness assessment of RC buildings by analysis of fragility and vulnerability

Miloš Čokić, Radomir Folić, Boris Folić
Article 106107

Article preview

Research article ○ Abstract only

Experimental investigation on elevated temperature mechanical properties in cast steel joints

Bin Qiang, Xing Liu, Hang Wu, Jun Wu, ... Yadong Li
Article 106158

Article preview

Research article ○ Abstract only

Experimental and FE analysis of the behavior of steel column base connections under tension and bending moment

Mahmoud T. Nawar, Ehab Matar, Ayman El-Zohairy, Ahmed Alaaser, Hassan Maaly
Article 106164

Article preview

Structures

Submit your article Guide for authors

View PDF Article preview

Research article Open access

Experimental and numerical evaluation of geometrical imperfection effects on the load bearing capacity of small-scaled voussoir arches

Davide Cassol, Giovanni Sommacal, Ivan Giongo, Gabriele Milani
Article 106101

View PDF Article preview

Research article Abstract only

Refinement in the understanding of confinement of concrete

Devesh K. Jaiswal, C.V.R. Murty
Article 106115

Article preview

Research article Open access

Design and testing of a self-centering friction damper-brace for compression ultimate limit state: Inelastic buckling

Seyed Mohamad Mahdi Yousef-beik, Sajad Veismoradi, Pouyan Zarnani, Pierre Quenneville
Article 106166

View PDF Article preview

Research article Abstract only

Static analysis of functionally graded porous beam-column frames by the complementary functions method

Hasibullah Rasooli, Ahmad Reshad Noori, Beytullah Temel
Article 106136

Article preview

Research article Abstract only

Bending performance of wet joints in negative moment zone of prefabricated small-box girder bridges: Experimental and numerical study

Jinsong Zhu, Zhouqiang Liu, Xiaoxu Liu, Lijuan Li, Yuzhen Li
Article 106103

Article preview

Research article Abstract only

An analytical and inverse analysis of the full-range behavior of embedded reinforcement based on a modified tri-linear bond-slip model

Faxiang Xie, Tianliang Chang, Geni Kuang, Feng Zhang

3269–3283]

Vijayakumar Natesan, Bharath Shanmugasundaram, Monish Sekar, Mahendrakumar Madhavan
Article 106106

View PDF

Research article ○ Abstract only

Experimental study on high-cycle fatigue behaviour of butt welds made of corroded AISI 304 stainless steel and Q460 high-strength steel

Ran Feng, Fuming Yang, Yongbo Shao, Krishanu Roy, ... Boshan Chen
Article 106141

Article preview

Research article ○ Abstract only

Comparative experimental studies on stiffened and unstiffened flange Cold Formed Steel welded sections using Cold Metal Transfer welding

Bishal Naik, Mahendrakumar Madhavan
Article 106140

Article preview

Research article ○ Abstract only

Assessment of purlins with paired torsion bracing in sloped roof systems: Direct strength method approach

Michael W. Seek, Onur Avci
Article 106157

Article preview

Research article ○ Abstract only

An experimental investigation and cost analysis of flexural or shear strengthening pre-damaged RC beams

Salih Aslan, İbrahim Hakkı Erkan, Ceyhun Aksoylu, Musa Hakan Arslan
Article 106091

Article preview

Research article *Open access*

Progressive collapse: Past, present, future and beyond

Nada Elkady, Levingshan Augusthus Nelson, Laurence Weekes, Nirvan Makoond, Manuel Buitrago
Article 106131

View PDF Article preview

Research article ○ Abstract only

Research article ○ Abstract only

Dynamic mechanical behavior of sandstone with filled joints at varying angles under coupled triaxial static and dynamic loading

Qingqing Su, Jinlong Cai
Article 106169

Article preview

Research article ○ Abstract only

Clinker storage silos: Validation of dynamic performance through measurements and finite element simulation

Łukasz Bednarski, Tomasz Howiacki, Rafał Sieńko
Article 106161

Article preview

Research article ○ Abstract only

Seismic behavior and initial rotational stiffness of beam-to-column composite connection in steel frame

Kang Ma, Xihao Ye, Ruoyang Wu, Haifeng Yu, ... Yang Zhao
Article 106069

Article preview

Research article *Open access*

A new generation of DCR by introducing reliability-survivability safety measure

Seyed Hooman Ghasemi, Ji Yun Lee, Andrzej S. Nowak
Article 106154

View PDF Article preview

Research article ○ Abstract only

Overstrength and plastic rotation of two-segment replaceable link with separated splicing plate

Shen Li, Yuanshuo Zhang, Ningjun Du, Yuanyuan Xia, Xiaolei Li
Article 106171

Article preview

Research article ○ Abstract only

Experimental study on performance of reinforced concrete short columns repaired and strengthened with Basalt fiber ultra-high-performance concrete (BF-UHPC)

Xuefeng Xu, Zongquan Jiang, Meixuan Wan, Sheng'ai Cui, ... Haonan Zeng
Article 106170

Article preview

Structures

Submit your article

Guide for authors

Investigation of mechanical behaviors of spoke-wheel cable structures through experimental and numerical analysis driven by digital-twin

Zhansheng Liu, Guoliang Shi, Yue Liu, Zhe Sun, ... T. Tafsirojjaman
Article 106099

Article preview

Research article ○ Abstract only

Experimental assessment of *sillar* masonry barrel vaults retrofitted with reinforced concrete elements

G. Caceres-Vilca, J. Copa-Pineda, F. Copa-Pineda, C. Málaga-Chuquitaype
Article 106145

Article preview

Research article ○ Abstract only

Distribution characteristics and simplified model of external explosion loading on large-scale doom-roof steel tanks

Zhen Wang, Ke Hu, Yang Zhao
Article 106150

Article preview

Research article *Open access*

Advancing ultimate bond stress–slip model of UHPC structures through a novel hybrid machine learning approach

Ahad Amini Pishro, Shiquan Zhang, Qixiao Hu, Zhengrui Zhang, ... Yuandi Zhao
Article 106162

View PDF Article preview

Research article ○ Abstract only

Identifying damage in long-span self-anchored suspension bridges using characteristic indices

Daihai Chen, Lijun Zhang, Zheng Li, Shizhan Xu, Yu Zhang
Article 106177

Article preview

Research article ○ Abstract only

Maximum permissible safe length of integral abutment bridges supported by steel H-piles

Yazan M. Alshawabkeh, Mohsen A. Issa
Article 106130

Article preview

Research article ○ Abstract only

Structures

Submit your article

Guide for authors

Structures

Submit your article | Guide for authors

Research article ○ Abstract only

Flexural behavior of novel marine concrete filled CFRP-aluminum alloy tube member

Zongping Chen, Weisheng Xu, Yuhan Liang, Linlin Mo, ... Ying Liang
Article 106184

Article preview

Research article ○ Abstract only

Study on mechanical properties of shotcrete lattice girder in a tunnel considering the excavation effect at early-age

Chuande Qi, Junfeng Liu, Shao Xing, Xianfeng Yin, ... Bingjun Sun
Article 106196

Article preview

Research article ○ Abstract only

Explicit equation for critical local buckling of thin walled FRP I-sections subjected to combined axial compression and bending

Rached Wafı, Ramzi Zakhama, Oualid Limam
Article 106167

Article preview

Research article ○ Abstract only

Investigation on effect of ECC coverage condition on seismic behavior of beam-column joint

Xinchen Zhang, Bing Li
Article 106195

Article preview

Research article ○ Abstract only

Critical load for shear-induced lateral-distortional buckling in I-section steel beams considering flexural stiffness ratio

Si-Ming Zhou, Gen-Shu Tong, Quan-Biao Xu, Hao-Chuan Zhu, Zhi-Bin Xiao
Article 106191

Article preview

Research article ○ Abstract only

Tensile behavior of a novel self-locking inter-module connection in modular steel buildings

Jiadi Liu, Jincheng Jiang, Yang Liu, Zhihua Chen, Kashan Khan
Article 106190

Article preview

Structures

Submit your article

Guide for authors

Research article ○ Abstract only

Two-way flexural behavior of biaxial voided slab using cuboidal shape of void formers

Abhijit J. Pawar, Yogesh D. Patil, Gaurang R. Vesmawala, Pravinchandra D. Dhake, Jagruti S. Nikam
Article 106175

Article preview

Research article ○ Abstract only

A comparative review study on the electrified road structures: Performances, sustainability, and prospects

Yaowen Pei, Feng Chen, Tao Ma, Gonghui Gu
Article 106185

Article preview

Research article ○ Abstract only

Interfacial debonding detection for steel-concrete composite structures part I: Benchmark test and signal calibration of contact and non-contact measurement

Hongbing Chen, Yaojun Ren, Shiyu Gan, Yuanyuan Li, ... Xin Nie
Article 106123

Article preview

Research article ○ Abstract only

Shaking table tests of power distribution cabinets: Physical damage, post-earthquake functionality and seismic response evaluation

Qingxue Shang, Haopeng Zuo, Xuebin Zhang, Zhen Li, ... Tao Wang
Article 106208

Article preview

Research article ○ Abstract only

Environmental life cycle costs of steel moment frames utilizing endurance time method

Ashkan Sedghi Moghadam, Mohammadreza Mashayekhi, Mohammad Sarcheshmehpour
Article 106207

Article preview

Research article ○ Abstract only

Cyclic behaviour of exterior bamboo scrimber beam-to-column connections

Shao-Bo Kang, Xiao-Fan Yu, Jun Xiong, Shu-Rong Zhou, Bin Long
Article 106173

Article preview

Structures

Submit your article

Guide for authors

Research article Abstract only

Risk assessment and prevention for typical railway bridge pier under rockfall impact

Zhiyang Cao, Zhanhui Liu, Guoji Xu, Han Lin, ... Nikolaos Nikitas
Article 106178

Article preview

Research article *Open access*

Multi-objective optimization of energy-dissipating steel plate fuse links using response surface method

Seyed Matin Goshtaei, Saber Moradi, Khandaker M. Anwar Hossain
Article 106224

View PDF Article preview

Research article Abstract only

Strengthening of two-way slabs with fiber-reinforced polymer composites: A new system using grooving technique and fans

Ala Torabian, Davood Mostofinejad
Article 106228

Article preview

Research article Abstract only

Experimental and numerical study of the flexural behaviour of semi-precast slab reinforced with prestressed FRP bars

Maha R.I. Mahmoud, Xin Wang, Mohamedelmujtaba Altayeb, Haithm A.M. Al-Shami, ... Amr M.A. Moussa
Article 106197

Article preview

Research article Abstract only

Seismic behavior of Q620 high-strength steel welded Box-section columns: Experimental tests, analysis, and model

Wenbing Han, Shidong Nie, Min Liu, Zhenye Chen, ... Mohamed Elchalakani
Article 106218

Article preview

Research article Abstract only

Automated operational modal analysis for supertall buildings based on a three-stage strategy and modified hierarchical clustering

Kun Zhao, Qiusheng Li, Mengmeng Sun, Shiji Huang, Xuliang Han
Article 106194

Article preview

Article preview

Research article ○ Abstract only

Machine learning-based modelling, feature importance and Shapley additive explanations analysis of variable-stiffness composite beam structures

Nikolaos Karathanasopoulos, Agyapal Singh, Panagiotis Hadjidoukas
Article 106206

Article preview

Research article ○ Abstract only

Fatigue test and service performance evaluation of high-speed train hanging equipment bolts

Tiantian Wang, Zhikang Zhang, Zhiguo Li, Jingsong Xie, ... Jingsong Yang
Article 106202

Article preview

Research article ○ Abstract only

Quantification of structural and non-structural robustness of tall steel buildings using a straightforward methodology

Mahyar Roshani
Article 106220

Article preview

Research article ○ Abstract only

Seismic behavior test and plastic hinge theory for HRB500 prefabricated steel reinforcement cage-cast-in-situ concrete columns

Zhong-wei Zhang, Guo-liang Bai, Fa-jiang Luo, Le-ping Ren, ... Shou-fu Li
Article 106213

Article preview

Review article *Open access*

FRP bar and concrete bond durability in seawater: A meta-analysis review on degradation process, effective parameters, and predictive models

Chiara Machello, Milad Bazli, Ali Rajabipour, S. Ali Hadigheh, ... Reza Hassanli
Article 106231

View PDF Article preview

Research article ○ Abstract only

Insight into the shear failure mechanism of Wound FRP reinforced concrete beams through numerical simulations considering interface damage and material anisotropy

Structures

Submit your article

Guide for authors

Research article ○ Abstract only

Numerical investigation of three-dimensional isolator and mitigation for single-layer lattice shell structure

Tianhao Yu, Zhenqin Huang, Chao Zhang, Weiyuan Huang, ... Yeyun Liu
Article 106235

Article preview

Research article ○ Abstract only

Experimental and numerical investigation on the buckling behavior of corroded CST under axial compression

Zhengyi Kong, Bo Yang, Cuiqiang Shi, Fan Yang, ... Quang-Viet Vu
Article 106192

Article preview

Erratum Full text access

Corrigendum to "Mechanical behavior of a novel steel-concrete joint in hybrid girder cable-stayed bridge" [Structures 57 (2023) 105239]

Lanting Zhao, Guangning Pu, Yangguang Yuan, Qi Guo, Yongliang Yu
Article 106139

View PDF

Research article ○ Abstract only

Development of beam elements for nonlinear analysis of reinforced concrete frames subjected to fire

Han-Soo Kim, Ha-Neul Choi, Tae-Hun Lim
Article 106229

Article preview

Research article ○ Abstract only

Performance evaluation of a seismic strengthening applied on a masonry school building by dynamic analyses

Mücahit Namlı, Fuat Aras
Article 106200

Article preview

Research article ○ Abstract only

Fail-safe topology optimization for a four-leg jacket structure of offshore wind turbines

Ruo Lan, Kai Long, Ayesha Saeed, Rongrong Geng, ... Jie Liu
Article 106183

Article preview

Structures

Research article ○ Abstract only

Crack _ PSTU: Crack detection based on the U-Net framework combined with Swin Transformer

Weizhong Lu, Meiling Qian, Yiyi Xia, Yiming Lu, ... You Lu
Article 106241

Article preview

Research article ○ Abstract only

Feasibility study of TSOB replacing standard high-strength bolt in T-stub connection

Yuzhu Wang, Lele Sun, Peijun Wang, Gangling Hou, ... Min He
Article 106246

Article preview

Research article ○ Abstract only

Cyclic performance of precast segmented bridge pier with inner column socket connection: A parametric study

Rashad Al-Shaebi, Mohammed Al-Haaj, Dan Zhang, Ning Li, Junfeng Jia
Article 106233

Article preview

Research article ○ Abstract only

Seismic fragility of vertically irregular gravity column-core tube structure subjected to pulse-like ground motions

Jun Wen, Haoran Xiong, Guobin Bu, Chong Xu, ... Jiaxin Wen
Article 106217

Article preview

Erratum Full text access

Corrigendum to “Finite element modeling of partially confined concrete and RC columns with embedded hexagonal-FRP strips under axial and horizontal loading” [Structures 54 (2023) 369–385]

Sonia Djenad, Mohamed Amin Bouzidi, Souad Ait Taleb, Abdelmadjid Si Salem
Article 106201

View PDF

Research article ○ Abstract only

Enhanced high-resolution structural crack detection using hybrid interacting Particle-Kalman filter

Md Armanul Hoda, Eshwar Kuncham, Subhamoy Sen
Article 106227

Article preview

Structures

Submit your article | Guide for authors

Research article ○ Abstract only

Experimental and numerical study of a metal-friction hybrid damper

Weizhi Xu, Yijie Cai, Ye Liu, Tianyang Zhang, Yujie Lu

Article 106256

Article preview

Page 1 of 2

Previous vol/issue

Next vol/issue

ISSN: 2352-0124

Structures 62 (2024) 106189

Contents lists available at ScienceDirect

Structures

journal homepage: www.elsevier.com/locate/structures

Stability design of cold-formed high and ultra-high strength steel thin-walled box sections using effective stress-strain model

Andy Prabowo [a], A.H.A. Abdelrahman [b,*], Yue-Yang Ding [c], Yao-Peng Liu [c]

[a] Department of Civil Engineering, Universitas Tarumanagara, Jakarta, Indonesia
[b] Structural Engineering Department, Faculty of Engineering, Mansoura University, Egypt
[c] Department of Civil and Environmental Engineering, The Hong Kong Polytechnic University, Hong Kong, China

ARTICLE INFO

Keywords:
Cold-formed steel
High strength steel
Effective stress-strain
Box sections
Direct analysis

ABSTRACT

This paper proposes an effective stress-strain model for integrated analysis and design of cold-formed steel structures with thin-walled sections. The study focuses on square and rectangular hollow sections made from high and ultra-high strength steel. Initially, a shell-finite element model (SFEM) was developed and validated using experimental data, specifically for cold-formed members subjected to axial compression. Subsequently, a comprehensive parametric study is conducted to establish the stress-strain relationship model through nonlinear finite element analysis. The proposed model incorporates material nonlinearity, cold-forming effect, local plate imperfection, and residual stresses into a unified stress-strain curve, leading to advanced structural analysis and design of cold-formed structures using simple one-dimensional beam-column element. Subsequently, the proposed method is then implemented in the conventional finite beam-column element analysis, demonstrating consistent agreement with both experimental tests and sophisticated finite shell element results. Finally, the robustness and validation of the proposed method are established, and its application is exemplified through the design of a modular integrated construction (MiC) structure. This study highlights the versatility and reliability of the proposed approach for the analysis and design of cold-formed steel structures.

1. Introduction

Cold-formed steel (CFS) structures have significantly influenced recent developments in steel construction, particularly in the context of Modular Integrated Construction (MiC) systems [1]. These structures offer numerous benefits, such as a high strength-to-weight ratio, ease of fabrication and mass production, rapid erection work, and excellent corrosion resistance [2]. It is worth noting that CFS members can exhibit enhanced strength compared to hot-rolled steel due to various manufacturing processes [3]. Rossi, et al. [4] have demonstrated that this strength enhancement is particularly notable in box sections (SHS and RHS), where the corner portions exhibit higher properties than the flat sections, rendering them particularly attractive in comparison to other CFS sections.

Research on the behavior of CFS box sections has reached a relatively advanced stage, with investigations of various steel grades. This observation is evident in the work of Gardner and Yun [5], who collated the results of the material property tests on various CFS grades. More recently, significant attention and efforts have been spent studying the behavior of cold-formed high-strength steel (CFHSS) members with a minimum grade of S700 [6–8]. Generally, high-strength steel (HSS) has a yield strength in the range of 350 MPa to 700 MPa, while ultra-high-strength steel (UHSS) typically exhibits a yield strength above 700 MPa. Interestingly, the current international design codes, such as AISC-360 [9], AISI [10], and EC3 [11], have not specified structural design guidelines for steel grades beyond 700 MPa. Therefore, there is still an opportunity to propose a novel design method that will be more practical and straightforward for engineers.

Currently, there is a limited availability of alternative design procedures for CFHSS box sections, especially when accounting for sections made from high- and ultra-high-strength steel. Ma et al. [12,13] recommend the traditional Effective Width Method (EWM) and also assess the feasibility of the more practical Direct Strength Method (DSM) [14]. These methods establish a relationship between the ultimate member strength and the cross-section slenderness, but they do not fully exploit the strain-hardening behavior of the material. Lan, et al. [15] advocate the Continuous Strength Method (CSM), which was initially developed for stainless steel structures. This method maximizes the

* Corresponding author.
E-mail address: a_hussain@mans.edu.eg (A.H.A. Abdelrahman).

https://doi.org/10.1016/j.istruc.2024.106189
Received 4 October 2023; Received in revised form 20 December 2023; Accepted 9 March 2024

utilization of the ultimate member deformation beyond the ultimate member strength [15,16]. Those few available design proposals mainly focus on a member capacity-based design with the member imperfections embedded in the design equations. Meanwhile, the corresponding member force and deformation demands are quantified based on the (amplified) first-order analysis as one of the second-order analysis approaches. Thus, they fit into the common practice of steel structure design, which still treats the structural analysis separately from the design work.

The use of "Direct Analysis Method" (DAM) seems to have not been popular in the CFS design so far. While this method has been extensively introduced in the design of hot-rolled steel, as seen in the American code [9] and Eurocode [11], its adoption in CFS design is still limited. The American Iron and Steel Institute (AISI) [10] has included DAM in its stability analysis requirement, but the overall approach still follows AISC-360 [9]. DAM is also often associated with the advanced analysis method since it automatically considers the member imperfections and connection deformations in the structural analysis. The advanced analysis aims to integrate the stability analysis and design process [17]. It brings a more consistent approach than the traditional effective length method (ELM) [18]. However, the current advanced analysis is only limited to compact sections since it relies on the development of a full plastic capacity of a cross-section. Exploring slender sections in a consistent advanced analysis framework, Gardner et al. [19] applied CSM strain limits to analyze hot-rolled steel I-shaped sections under major-axis bending. Nevertheless, non-compact and slender sections are easily found in the CFS structures, which are typically failed due to local buckling with the ultimate resistance below the plastic limit. Formerly, the effect of local buckling on the beam-column analysis of box sections was studied by Shanmugam, et al. [20] and Chan, et al. [21]. In their nonlinear finite element analysis, a stress-strain relationship of a plate under compression was utilized to consider the local buckling. Thus, these studies treated a box section as per plate decomposition rather than a unified single cross-section behavior.

Recently, Modular Integrated Construction (MiC) has gained significant attention due to its prefabricated nature, enabling higher precision and faster erection compared to conventional frame-type structures [22–24]. For example, numerous MiC projects have been undertaken in Hong Kong, with a substantial portion consisting of steel MiC structures, primarily with less than six floors, serving as advanced housing solutions or nursing facilities [25–27]. However, the application of such structures in Hong Kong faces challenges due to transportation limitations. Given that the average weight of steel MiC structures is approximately 20 tonnes, this scenario highlights the judicious choice of utilizing high-strength cold-formed steel for low-rise MiC structures. The corner posts of such MiC structures are generally square hollow sections or cold-formed steel angles (3 mm to 4 mm) [28,29]. This variability in cold-formed steel sections allows for tailored utilization based on the specific module type, thereby affording design versatility and weight reduction.

To address the aforementioned challenges, this paper aims to promote the application of DAM for CFS structure. This method is suitable for both non-slender and slender cross-sections and incorporates considerations for local buckling within the proposed analysis framework. Firstly, an effective stress-strain material model was developed through a comprehensive parametric study focused on the CFHSS box sections under consideration. This study also adopted the principle of mimicking local buckling through a constitutive model. However, a much broader extension was implemented by taking into account the residual stress and cold-forming effect in the constitutive model. More importantly, the constitutive model was developed based on a unified single cross-section behavior rather than plate decomposition. Hence, the model is named an effective stress-strain relationship. The relationship is used to include the material nonlinearity in the DAM, which utilizes a line-based beam-column element.

2. Effective stress-strain relationship

Initially, the effective stress-strain relationship has been recommended to design a non-compact and slender concrete-steel composite member. Lai and Varma [30] developed the relationship to analyze a non-compact and slender concrete filled-tube (CFT) members. It was demonstrated that shell finite element models (SFEM) for CFT stub columns were developed to predict the normalized stress versus normalized strain relationship of rectangular and circular CFT. The sections had cross-section slenderness between 60 and 100, whereby the local buckling dominated the failure of the stub columns. Plate imperfection, residual stress, strain hardening, and concrete confinement were incorporated into the SFEM analysis. Therefore, the proposed relationship was named an effective stress-strain relationship.

Lai and Varma [30] used the developed model for a member analysis using the fiber sectioning method. The algorithm was created to prove that their proposed relationship and the numerical model of a CFT beam-column could match against the test results. In another study, Du, et al. [31] introduced the DAM for slender CFT sections by implementing Lai and Varma [30] stress-strain relationship to consider the material nonlinearity. Du, et al. [31] utilized the effective stress-strain relationship to account for distributed plasticity along the member length by using the fiber discretization technique. This technique is suitable for a second-order analysis using an advanced beam-column element, which was established by Du, et al. [17]. The outcome from the latter study has been added to the last version of NIDA software [32]. Hence, it can be concluded that an effective stress-strain model performs well in the analysis using the fiber discretization method.

Another application of an effective stress-strain model can be found in the numerical modelling for stability design of angle structures proposed by Abdelrahman, et al. [33]. This study generated the effective stress-strain model from shell finite element analysis (SFEA) results. Flexural and flexural-torsional buckling modes were considered and captured in the model. The proposed relationship has considered global member imperfection and residual stress. Stub column failure was excluded in the development since it seems rare to find this case in the application of angle structures. Local buckling failure mode was excluded therein since it is not intended to design a short column. With the proposed model, the analysis and design of angle structures can be unified without calculating the flexural torsional buckling capacity from a separate design equation. For the validation of the stress-strain model, the analysis results from Abaqus [34] using 1D-line and shell elements were compared with test results. The proposed effective stress-strain model was also used to analyze a truss structure wherein the results were also validated against test results. The results showed that the effective stress-strain model embedded in 1D-line element analysis predicted the outcome of shell element analysis well. Indeed, SFEA is more powerful since member imperfections and various failure modes (e.g., torsional-buckling) can be explicitly and effectively modelled. Such complexities and uncertainties may not be taken into account when using 1D line elements in the analysis. As such, LFEA (line finite element analysis) has relatively faster and cheaper computational efforts. Overall, Abdelrahman, et al. [33] proved that the effective stress-strain model could be implemented in available commercial software for a more advanced system-based analysis.

3. Finite element modeling

According to the existing studies [30,33], the SFEA was conducted as the first step to obtain an effective stress-strain model. Like Lai and Varma [30], SFEA of CFHSS stub columns was also developed in this study, simulating local buckling failure modes of a pure compression member. The FEA results were verified using the test result reported by Ma, et al. [35] and Wang, et al. [8]. The local buckling failure was dominant in these two test results, which was also reflected in the load versus deformation (corresponding to the stress-strain) curves generated

Table 1
Ultimate strength ratio between experiment (P_{Exp}) and FEA (P_{FEA}) results.

Reference	Specimen	Steel Grade	Imperfection magnitude			
			Actual measurement	$a/200$	$a/400$	Dawson and Walker[39]
Ma, et al.[35]	H80 × 80 × 4	S700	1.05	1.08	1.05	1.04
	H100 × 100 × 4	S700	1.03	1.10	1.05	1.02
	H120 × 120 × 4	S700	0.99	1.08	1.02	0.99
	H140 × 140 × 5	S700	1.02	1.06	1.01	1.01
	H140 × 140 × 6	S700	1.00	1.05	1.01	0.99
	H160 × 160 × 4	S700	1.03	1.04	1.02	1.02
	H100 × 50 × 4	S700	1.01	1.01	1.00	0.98
	H200 × 120 × 5	S700	1.00	1.02	1.00	1.00
	V80 × 80 × 4	S900	1.09	1.11	1.07	1.07
	V100 × 100 × 4	S900	1.03	1.06	1.00	1.01
	V120 × 120 × 4	S900	1.03	1.05	1.01	1.02
Mean			1.03	1.06	1.02	1.01
CoV			0.03	0.03	0.02	0.02
Wang, et al.[8]	SHS200 × 200 × 4	S500	0.97	0.99	0.97	0.97
	SHS200 × 200 × 5	S500	1.06	1.09	1.05	1.03
	SHS150 × 150 × 4	S700	1.00	0.97	0.94	0.95
	SHS110 × 110 × 4	S700	1.09	1.08	1.02	1.01
	SHS100 × 100 × 4	S960	1.11	1.02	1.01	1.00
	SHS120 × 120 × 4	S960	1.01	1.00	0.98	0.99
	SHS120 × 120 × 3	S960	0.97	0.96	0.97	0.97
	SHS150 × 150 × 7	S960	1.31	1.25	1.19	1.16
Mean			1.04	1.03	1.00	1.00
CoV			0.05	0.05	0.04	0.04

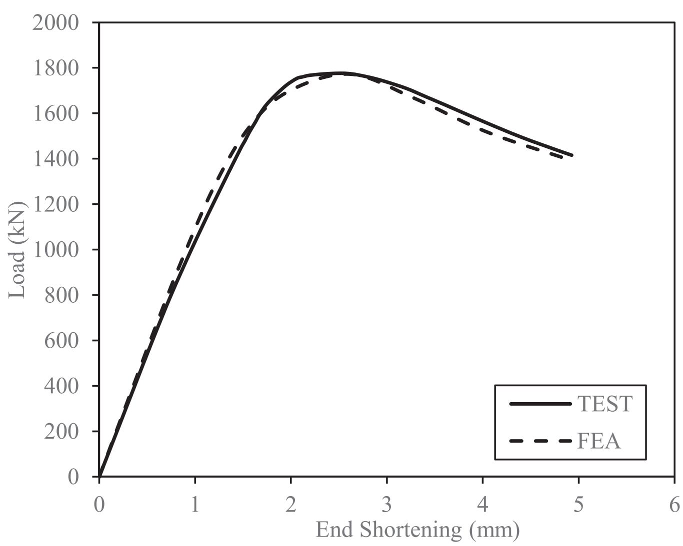

Fig. 1. Verification of load-end shortening curves for specimen H200 × 120 × 5 [35].

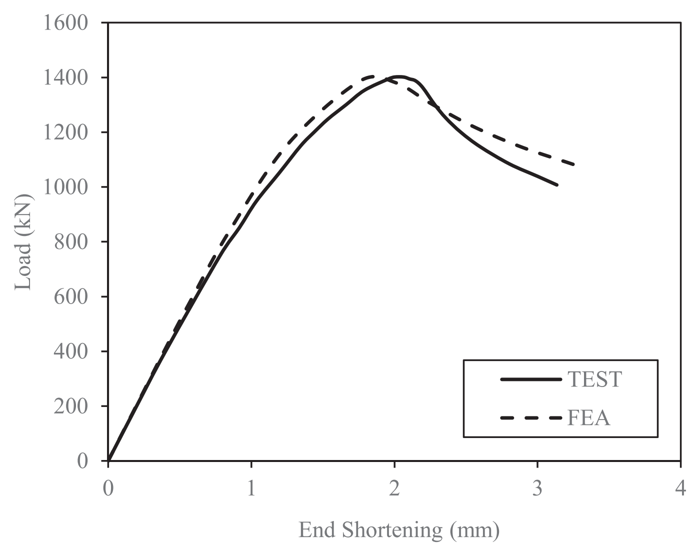

Fig. 2. Verification of load-end shortening curves for specimen V100 × 100 × 4 [35].

from FEA. The outcome of the proposed model from this study is expected to be used in conjunction with the force-based beam-column element that occupies the fiber discretization method.

The finite element model based on Abaqus [34] utilizes the shell element (S4R) due to its satisfactory performance in simulating the cross-sectional local buckling [13,36,37]. The element size was then determined based on the (B+H)/40 value, where B and H were the flange and web widths of CFHSS, respectively. Measured material properties by Ma, et al. [6], and plate imperfections reported by Ma, et al. [35] were adopted in the FE model. Three amplitudes were used for initial geometric imperfections, as indicated by Yun and Gardner [38]. These included a/400, a/200, and an empirical formula by Dawson and Walker [39]. The latter formula is shown in Eq. (1), wherein the updated critical local buckling stress from Seif and Schafer [40] (Eq. (2)) was used.

$$\omega_o = 0.068t\frac{f_y}{f_{cr}} \tag{1}$$

$$f_{cr} = 4\left(\frac{B-t}{H-t}\right)^{1.7}\frac{\pi^2 E}{12(1-\nu^2)}\left(\frac{t}{B-t}\right)^2 \tag{2}$$

The effect of residual transverse residual stress was excluded in the SFEA as it was negligible based on several studies [12,15,41]. In contrast, bending residual stress was considered and incorporated into the material properties test. According to the proposed FEM of Ma, et al. [12], the stress-strain curve obtained from the corner tensile coupon test was assigned to the corner part with a 2 t (2 times the section thickness) extension into the flat portion of the box section. A fixed-ended boundary condition was applied at the two ends through a reference point. An Eigen buckling analysis was first conducted, and the resulting buckling modes were scaled as initial geometric imperfections within the nonlinear static RIKS analysis in the second step.

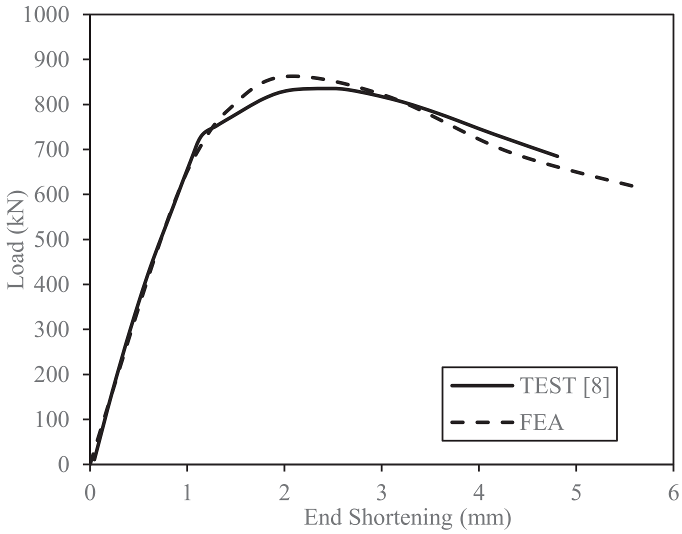

Fig. 3. Verification of load-end shortening curves for specimen SHS 120 × 120 × 3 [8].

The ultimate loads obtained from the SFEA were compared with the test results, as tabulated in Table 1. It is clearly seen that the predicted ultimate loads from SFEA were generally in good agreement with the test results. Moreover, the most accurate results were obtained when the imperfection magnitude from a modified Dawson and Walker [39] empirical formula is imposed. Meanwhile, the load-axial shortening curves from the FEA were sufficiently close to the test curves, as shown in Fig. 1, Fig. 2, and Fig. 3. In addition, Fig. 4 shows a comparison of the typical failure mode obtained from the test and FEA. Overall, the developed FEM is reliable and can be used for a parametric study.

4. Development of effective stress-strain model for CFHSS

4.1. Scope and limitations

An extensive parametric study was conducted to develop an effective stress-strain model for CFHSS, involving 105 square hollow sections (SHSs) and 108 rectangular hollow sections (RHSs). Three sets of yield stress (f_y) and Young's modulus (E) were selected from the test results of Ma, et al. [6], as collected in Table 2. Meanwhile, Table 3 presents the list of sections and the various parameters considered to develop the effective stress-strain model. The corner radius (r) was equal to the thickness (t) when t was smaller than 7 mm, and r was equal to 1.5t for sections with $t \geq 7$ mm. The normalised section slenderness (λ_n) of a section was calculated from Eq. (3). This variable becomes a vital parameter to control the scope of the parametric study. Ma, et al. [13] claims that elastic local buckling failure will exhibit when λ_n value is higher than 1.28.

$$\lambda_n = \frac{b}{t}\sqrt{\frac{f_y}{E}} \tag{3}$$

Table 2
Material properties for parametric study.

Steel Grade	f_y (MPa)	E (GPa)
S700	719	212
S900	982	208
S1100	1073	205

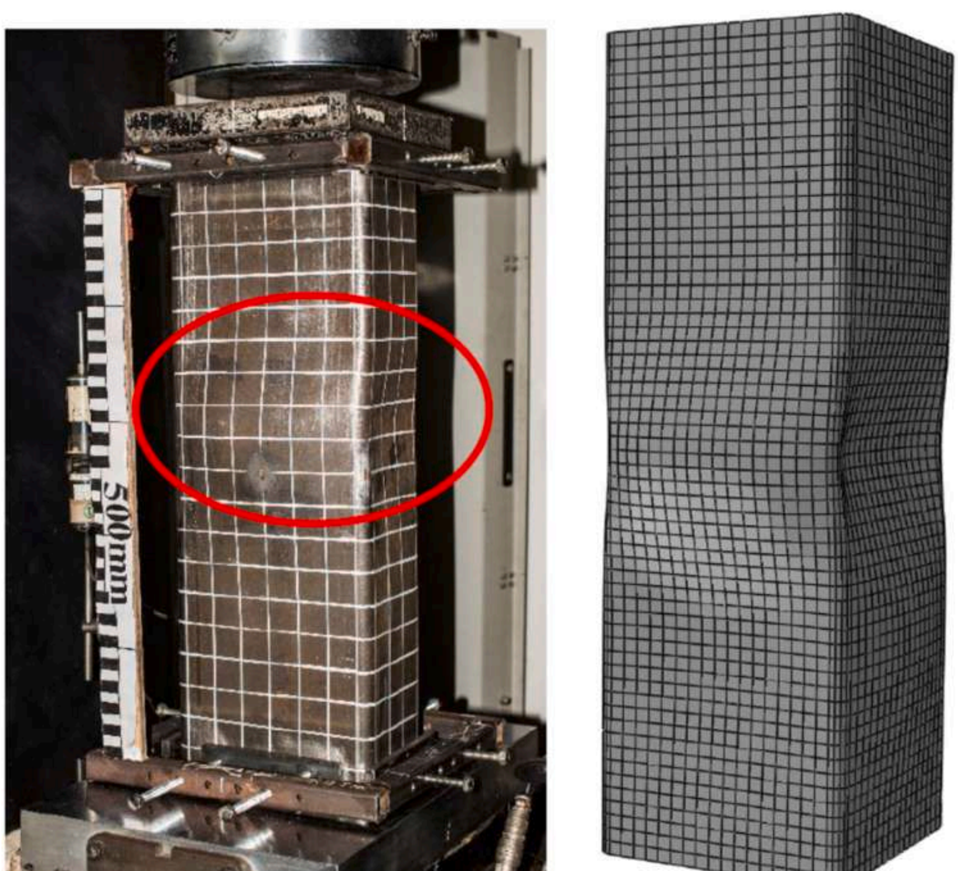

Fig. 4. Comparison of failure modes between a test result (left) [13] and FEA (right).

Table 3
Parametric study of SHS and RHS.

Cross-section	$H \times B$ (mm)	t (mm)	λ_n		
			S700	S900	S1100
SHS	300 × 300	3, 3.5, 4, 5, 6, 8, 10	1.46 – 5.59	1.72 – 6.6	1.81 – 6.95
	270 × 270	3, 3.5, 4, 5, 6, 8, 10	1.28 – 5.01	1.51 – 5.91	1.59 – 6.22
	250 × 250	3, 3.5, 4, 6, 8, 10	1.16 – 4.62	1.37 – 5.45	1.45 – 5.74
	220 × 220	3, 4, 5, 10	0.99 – 4.04	1.17 – 4.76	1.23 – 5.02
	200 × 200	3, 3.5, 5, 6, 10	0.87 – 3.65	1.03 – 4.31	1.23 – 5.02
	180 × 180	3.5, 10	0.76, 2.76	0.89, 3.26	0.94, 3.43
	150 × 150	3.5, 10	0.58, 2.26	0.69, 2.67	0.72, 2.81
	120 × 120	3.5, 6	0.93, 1.76	1.1, 2.08	1.16, 2.19
RHS	300 × 180	3, 3.5, 4, 5, 6, 8, 10, 12	1.16 – 5.59	1.37 – 6.60	1.45 – 6.95
	270 × 150	3, 3.5, 4, 5, 6, 8, 10	1.28 – 5.01	1.51 – 5.91	1.59 – 6.22
	250 × 120	3, 3.5, 4, 6	2.19 – 4.62	2.59 – 5.45	2.73 – 5.74
	220 × 120	3, 4, 5, 10	0.99 – 4.04	1.17 – 4.76	1.23 – 5.02
	200 × 100	3, 4, 5, 6, 10	0.87 – 3.65	1.03 – 4.31	1.23 – 5.02
	180 × 100	3.5, 10	0.76, 2.76	0.89, 3.26	0.94, 3.43
	150 × 100	3.5, 10	0.58, 2.26	0.69, 2.67	0.72, 2.81
	120 × 100	3.5, 6	0.93, 1.76	1.1, 2.08	1.16, 2.19

In developing the effective stress-strain model, both studies [30,33] agreed that the proposed model had to be conservative. Furthermore, these studies [30,33] also stated that developing a model that precisely simulates all the loading conditions was impractical. The fundamental behavior of steel plates under pure compression was considered by analyzing the stub columns. An elastic-rigidly plastic model has been selected for the constitutive relationship on the tension fiber for tensile action.

4.2. Model development

The effective stress-strain model proposed in this study has considered the following aspects:

- Strength enhancement due to cold-working process.
- Bending residual stress.
- Elastic and inelastic local buckling.
- Geometric imperfections.

The model can be used to simulate material nonlinearity in the analysis in combination with the application of the 1D beam-column element developed by Du, et al. [17]. The idea behind this study was to bring the generalized results of shell FEA of a short member into the 1D finite element analysis of a long beam-column member.

The effective stress-strain model accounts for all sources of nonlinearity, including both material and geometric factors. The design obtained from the nonlinear analysis can optimize the structural performance even though the strength limit is achieved. With the proposed model, the design of a slender section can be more optimum due to the mobilization of post-buckling capacity. This principle differs from the current practice, which focuses on using first-order analysis and compact sections. The second-order effect is usually considered by using amplification and or additional notional loads. Meanwhile, material nonlinearity is considered by using a reduction factor applied to Young's modulus as specified in AISC-360 [9].

The recommended effective stress-strain model was extracted from results analyzed using four-node shell element S4R in ABAQUS. The load versus end-shortening curve from the analysis outcome was converted to a normalized compressive stress-strain relationship (σ - ε). Compressive stress (σ) was obtained by dividing the load capacity with the cross-sectional area (A), and the compressive strain (ε) was calculated by dividing the end-shortening with the stub column length (L). Due to the consideration of short column failure, L was equal to three times the nominal section size (B). For RHS, the average between larger (H) and smaller (B) section sizes was used to calculate L. Both compressive stress and strain values were then normalized to yield stress and yield strain, respectively. As a result, the normalized stress-strain for various slenderness (b/t) and f_y is presented in Fig. 5.

From Fig. 5, it can be observed that as the section becomes more slender, the normalized compressive stress factor (σ/f_y) significantly decreases and is well below 1. It was assumed that buckling took place once the ultimate load was achieved. Elastic local buckling would be the typical failure mode if a section buckled under the yield stress. In all figures, none of the sections reached inelastic local buckling. Apart from section slenderness, the effect from f_y was also seen. The ultimate compressive stress decreases when f_y increases. This trend was also similar to the finding in [33] and [30]. Finally, it was observed that the member's buckling behavior was influenced by the b/t ratio. As the b/t ratio increased, the strength degradation became more gradual compared to the less slender section. It can be conjectured that the strength degradation correlated with the failure mode, as illustrated in Fig. 6. For the most slender section (b/t = 96), local buckling was uniformly spread throughout the length, while for the most stocky section (b/t = 25), local buckling was concentrated at the mid-length. For the three figures in Fig. 5, it was observed that the post-buckling strength degradation became gradually constant when the compressive strain reached four times the yield strain ($4\varepsilon_y$).

Based on the parametric study, the compressive stress-strain curve could be simplified into the trilinear curve, as illustrated in Fig. 7. Three critical points were marked in the curve comprised of the peak buckling stress (σ_p), post-buckling stress limit (σ_2), and secant modulus stiffness before buckling (E_s), and plotted in a nondimensional format. These three variables are also recommended by Abdelrahman, et al. [33]. The secant modulus was chosen over a tangent modulus, as the model should be conservative and straightforward for application. E_s is used to calculate the strain at $4\varepsilon_y$.

The normalized buckling stress from the FEA versus the λ_n is plotted in Fig. 8. From the figure, it can be observed that there was a consistent trend between the decreasing of buckling load with the increasing of slenderness. By using regression analysis, an equation of the trendline was formed. All of the equations were developed based on the "Power" format. This format was relatively simple and easy to maximize R^2 value close to 1. The peak of normalised buckling stress for SHS and RHS sections is written in Eq. (4) and Eq. (5), respectively. For RHS sections, an additional variable was added to consider the aspect ratio.

$$\frac{\sigma_p}{f_y} = 1.19(\lambda_n{}^{-0.75}) \leq 1.0 \tag{4}$$

$$\frac{\sigma_p}{f_y} = 1.09(\lambda_n{}^{-0.67})\left[\frac{H}{B}\right]^{0.35} \leq 1.0 \tag{5}$$

For sections with λ_n less than 1.28, the peak buckling stress was limited to 1. The factor of 1.28 was a limit between elastic local buckling and inelastic local buckling based on Ma, et al. [35]. The peak stress was limited to yield stress for a conservative approach. Experiment results showed that when inelastic local buckling occurred, the failure stress would be higher than the yield stress. This can be seen in Fig. 8(a) and (b), whereby there were several peak stress values higher than 1 for λ_n

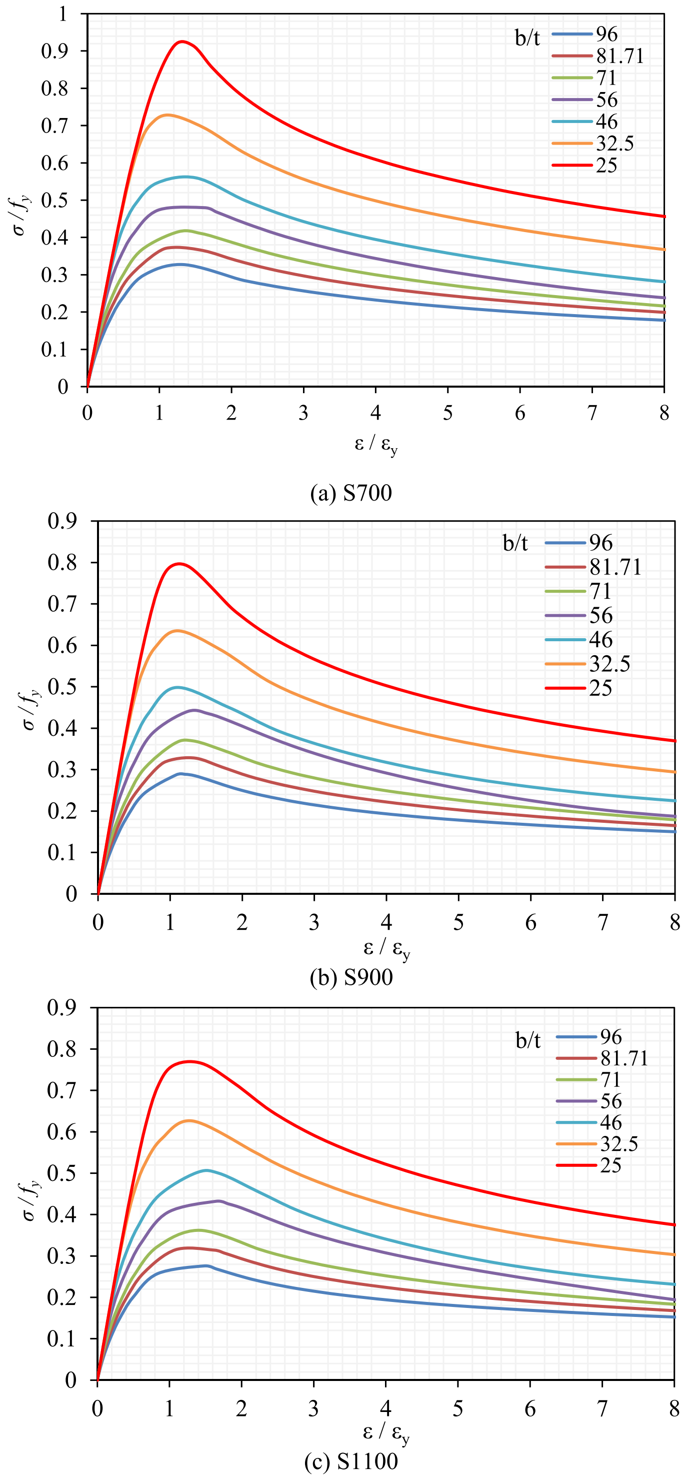

Fig. 5. Normalised compression stress-strain of SHS.

less than 1.28.

The strain at peak stress was approached by calculating the secant modulus of elasticity (E_s) since it would be relatively simple because the original compressive stress-strain curve from FEA was nonlinear. The E_s was normalized to Young's modulus to have a consistent form with the other parametric equations. The trend of normalized E_p values with λ_n closed to the Eq. (6) and Eq. (7). The trendlines were drawn in Fig. 9, together with the results obtained from the parametric study. It was realized that the results were more scattered than the peak stress. However, Eq. (6) and Eq. (7) were the best results from the regression analysis model; R^2 is more than 0.79 for those equations.

$$\frac{E_s}{E} = 0.94\left({\lambda_n}^{-0.78}\right) \tag{6}$$

$$\frac{E_s}{E} = 0.86\left({\lambda_n}^{-0.68}\right)\left[\frac{H}{B}\right]^{0.35} \tag{7}$$

Another important parameter in Fig. 7 is the post-buckling stress limit (σ_2). As mentioned, the compressive stress would decrease slightly once the strain reached $4\varepsilon_y$. Simply speaking, the stress would be

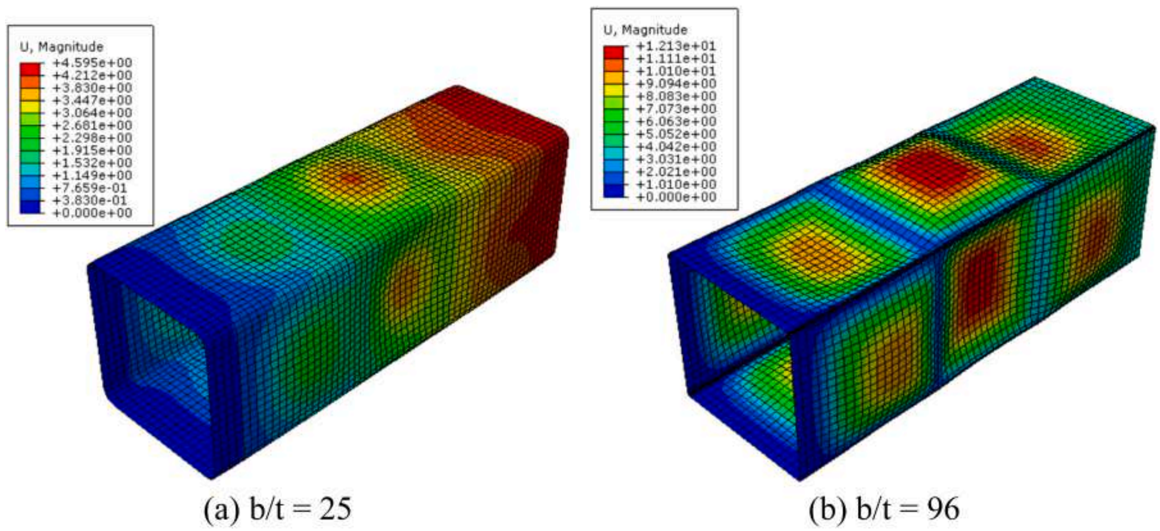

Fig. 6. Failure mode of a stub column.

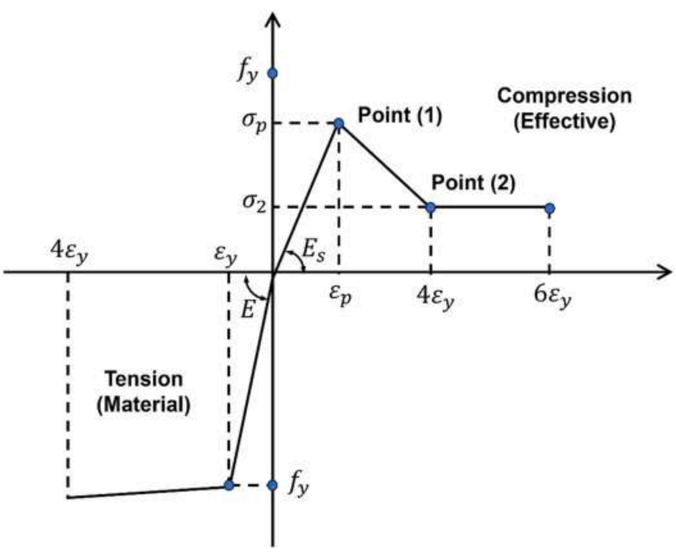

Fig. 7. Effective stress-strain model for CFHSS.

constant from this point onward. From the parametric study, σ_2 was plotted against λ_n as described in Fig. 10. A trendline was drawn in the two figures, and an equation was formed. Eq. (8) and Eq. (9) were the trendline equations for the different cross-sections. Again, the stress obtained from these equations was constrained to f_y for conservative design, as it could potentially exceed f_y for stocky sections.

$$\frac{\sigma_2}{f_y} = 0.83\left(\lambda_n^{-0.75}\right) \leq 1.0 \tag{8}$$

$$\frac{\sigma_2}{f_y} = 0.93\left(\lambda_n^{-0.8}\right)\left[\frac{H}{B}\right]^{0.3} \leq 1.0 \tag{9}$$

Since all the parameters in the proposed stress-strain model have been explored, the next stage is to calibrate the model with the experiment results. The application of the proposed model to the member design will also be presented in the following part. It is also interesting to verify the results with the member test results.

5. Application of effective stress-strain model

This section aims to validate the proposed stress-strain relationship for predicting the behavior of CFS box sections made from high-strength steel. Additionally, it explores the validity of the proposed 1D beam-column element approach for nonlinear collapse analysis of steel members with CFS box sections. Experimental results and those generated from sophisticated finite shell element models are used for

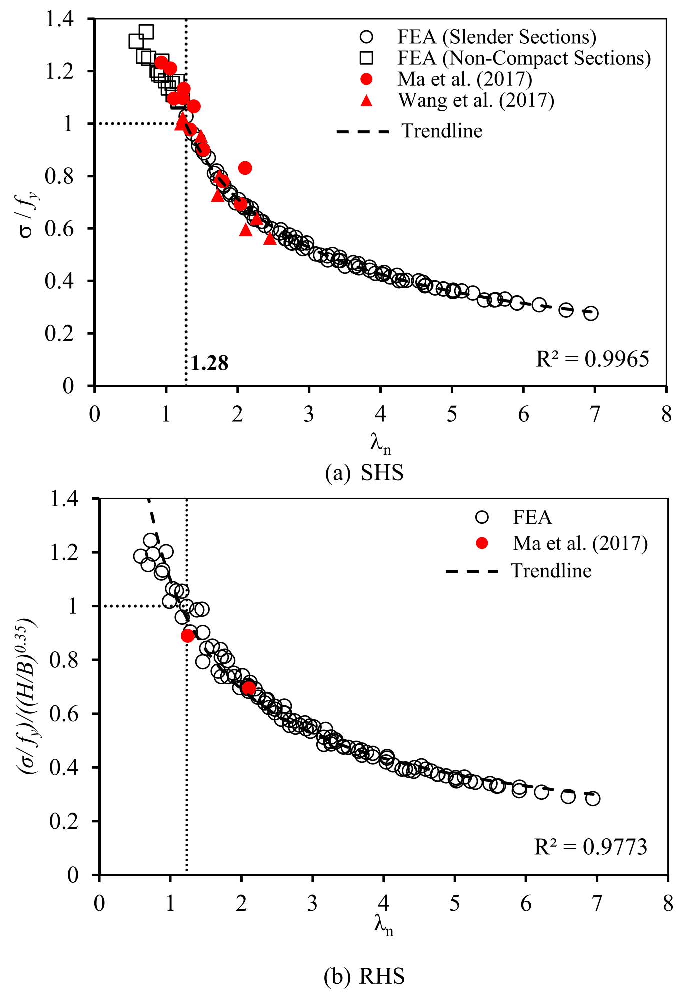

Fig. 8. Relationship between normalized buckling stress and λ_n.

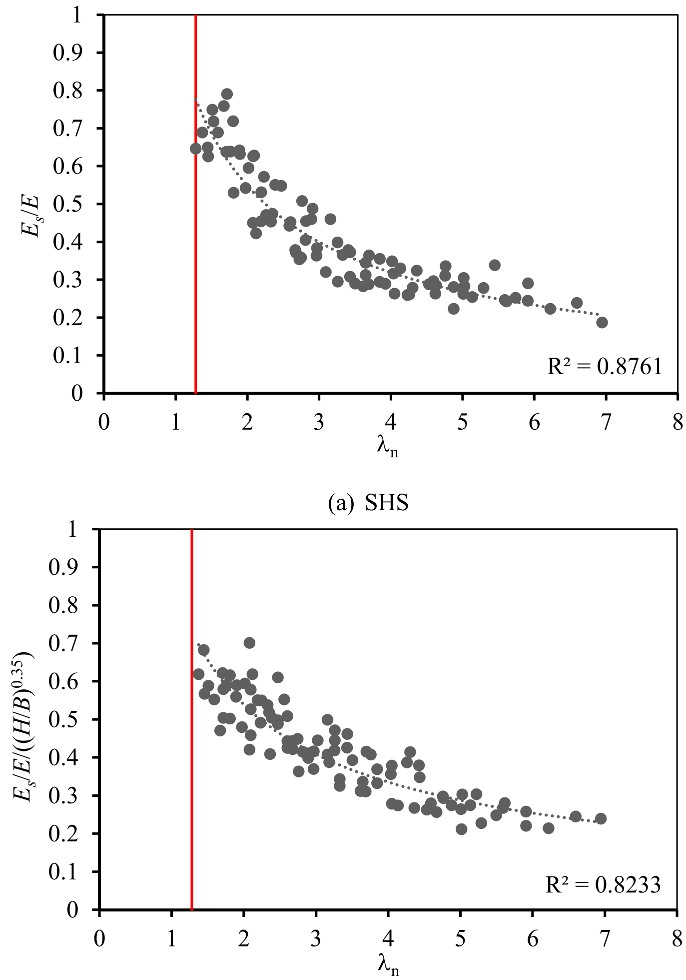

(a) SHS

(b) RHS

Fig. 9. Relationship between secant modulus (E_s) and λ_n.

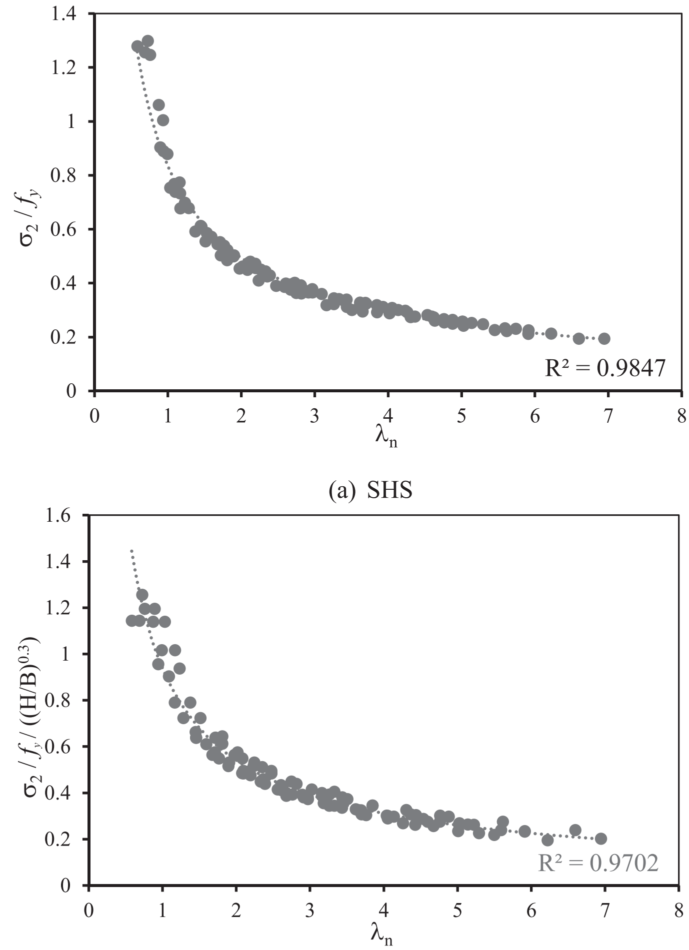

(a) SHS

(b) RHS

Fig. 10. Relationship between normalized σ_2 and λ_n.

verifications and validations. With these purposes, the proposed stress-strain relationship is implemented within the B31 beam-column element in ABAQUS, using the scripting technique [42–44] that imposes the proposed curve as a constitutive material model.

In order to conduct comprehensive comparison studies, the following four sets of results are analyzed: 1) 1D line FE models with the proposed stress-strain relationship (implicitly accounting for imperfections), denoted as LFEMI; 2) 1D line FE models with the material stress-strain relationship (with no allowance for material or geometric imperfections), denoted as LFEM; 3) the sophisticated shell FE models (SFEM); and 4) the experimental tests.

Finally, a modular integrated construction (MiC) structure is designed to demonstrate the versatility and reliability of the proposed approach for the analysis and design of cold-formed steel structures.

5.1. Comparisons between the simplified 1D line element method and shell FE models

This example demonstrates comparisons between results obtained from sophisticated SFEM and the proposed LFEMI for collapse analysis of CFS members made from box sections. Herein, the analysis matrix includes a wide range of cross-section dimensions as summarized in Table 4: (a) cross-sectional width $B = 70 - 400mm$; (b) width-to-thickness ratio $B/t = 15 - 200$ for slender sections; (c) yield stress $F_y = 500 - 1100MPa$ for high-strength steel; and (d) slenderness coefficient $\lambda_n = 1.25 - 10$. Note that the influence of initial imperfections is

Table 4
Analysis matrix for CFS hollow box sections.

No. of specimens	$B(mm)$	$t(mm)$	B/t	$F_y(MPa)$	$\lambda_n = \frac{B}{t}\sqrt{\frac{f_y}{E}}$
100	70 to 400	1 to 9	15 to 200	500 to 1100	1.25 to 10

included via the proposed effective stress-strain model. The ultimate loads obtained from the two methods (i.e., SFEM and LFEMI) are normalized by dividing those loads by the corresponding squash load ($P_y = A * F_y$); accordingly, they are plotted in Fig. 11(a) for comparison. Results from the LFEMI are within 10% below those obtained from sophisticated SFEM on the conservative side.

On the other side, showing that the analysis matrix includes a wide practical range of CFS members, Fig. 11(b) depicts the predicted LFEMI-to-SFEM ratios versus the slenderness coefficient (λ_n). The slenderness coefficient mostly varies between 1 and 4.5, while a few members have a high B/t ratio for slender sections. The mean LFEMI-to-SFEM ratio is 0.94, with a relatively low coefficient of variance (COV) of 0.03. It becomes clear that developing an effective stress-strain relationship that implicitly accounts for cross-sectional geometric imperfections is crucial for more accurate results, thereby adopting LFEMI for a practical design of CFS structures comprising box sections. The proposed stress-strain relationship can precisely simulate the cross-sectional buckling

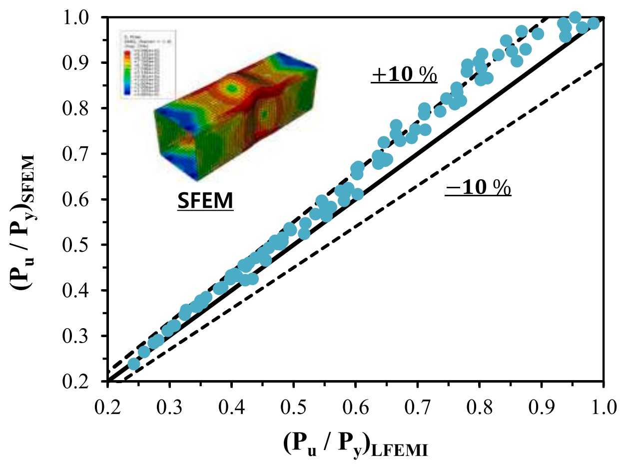

(a) Normalized ultimate loads obtained from LFEMI vs. SFEM

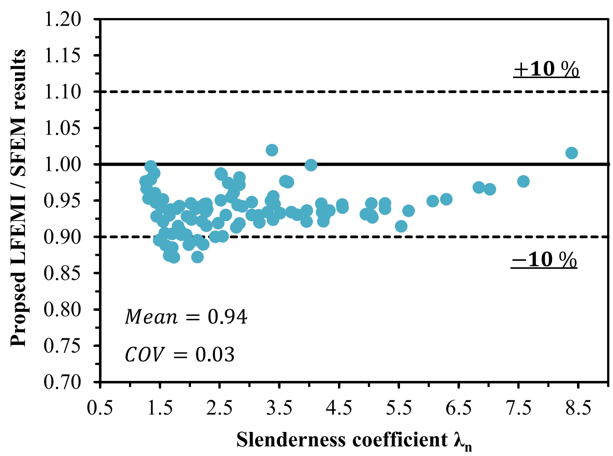

(b) LFEMI / SFEM results vs. slenderness coefficient λ_n

Fig. 11. Comparisons between LFEMI results and SFEM.

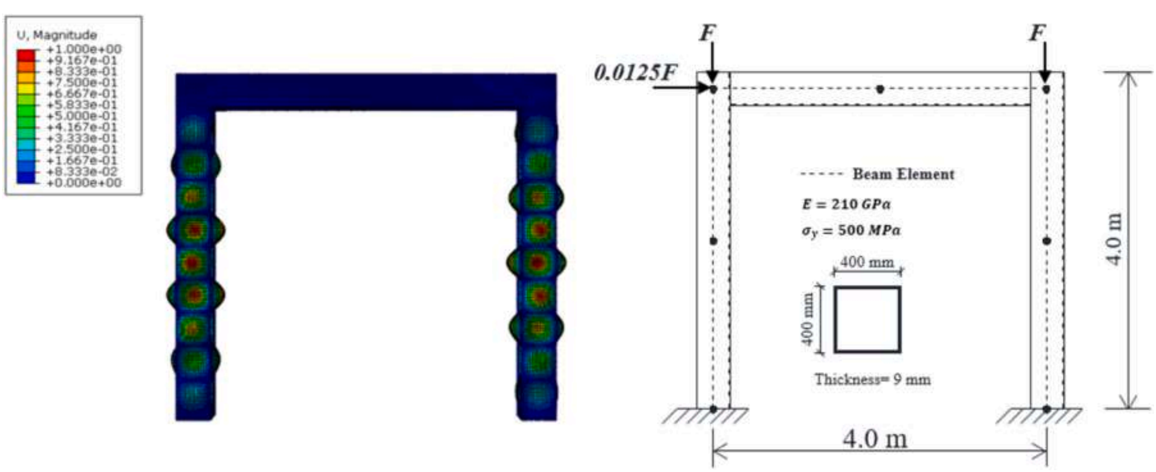

Fig. 12. The configuration of a single-span portal frame comprising CFS box sections.

behavior for advanced analysis.

To further examine the proposed approach for a second-order inelastic analysis of CFS structures comprising CFS box sections, the proposed stress-strain relationship is implemented within the LFEM to analyze a single-span portal frame subjected to vertical and lateral loads. The geometric configurations, including dimensions, loading, and boundary conditions, are plotted in Fig. 12, together with the Eigen-buckling mode for geometric imperfections within SFEM. The portal frame is assembled with CFS square hollow sections (SHS) with outside dimensions of 400 mm and a wall thickness of 9.0 mm, making the cross-sectional slenderness $B/t = 44.44$, whereby the local buckling dominated the failure mode. The Young's modulus, Poisson's ratio, and

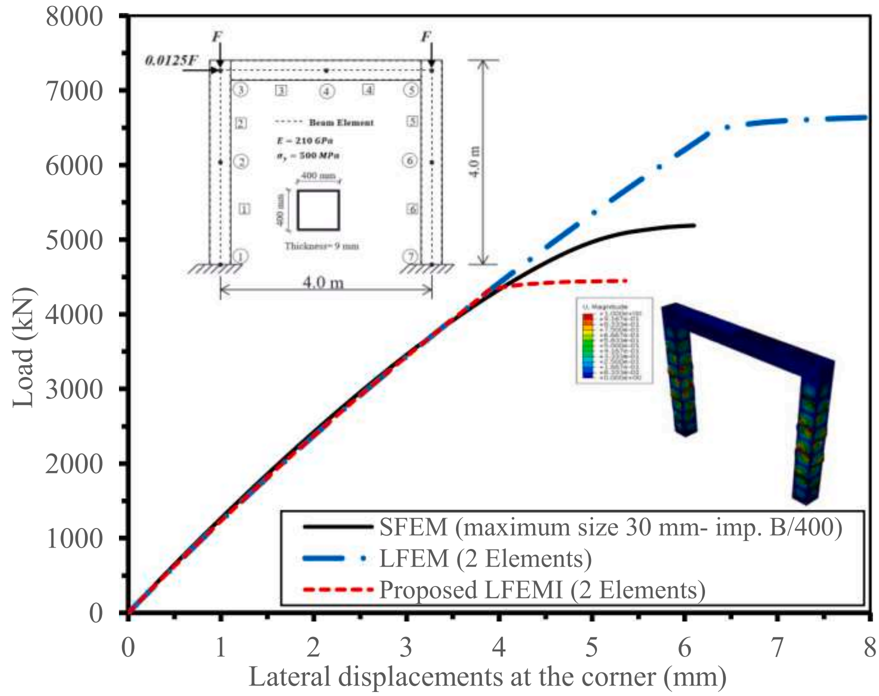

Fig. 13. Load-displacement curves for a portal frame comprising CFS box sections.

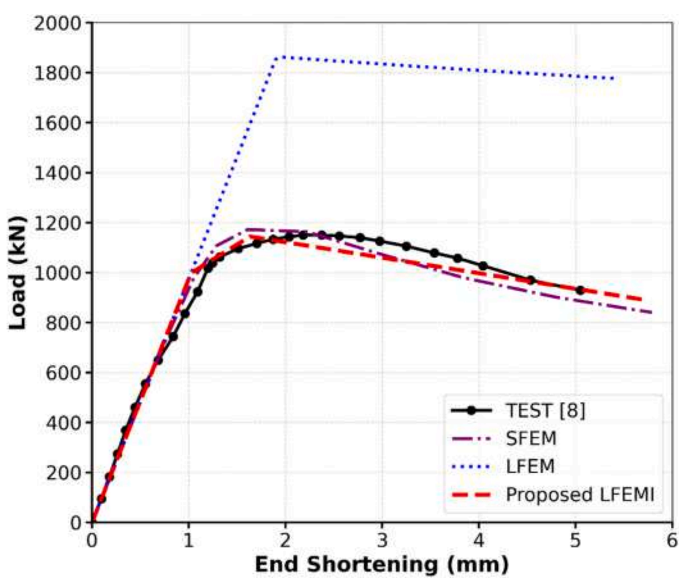

Fig. 14. Verification of load-end shortening curves SHS 120 × 120 × 3.

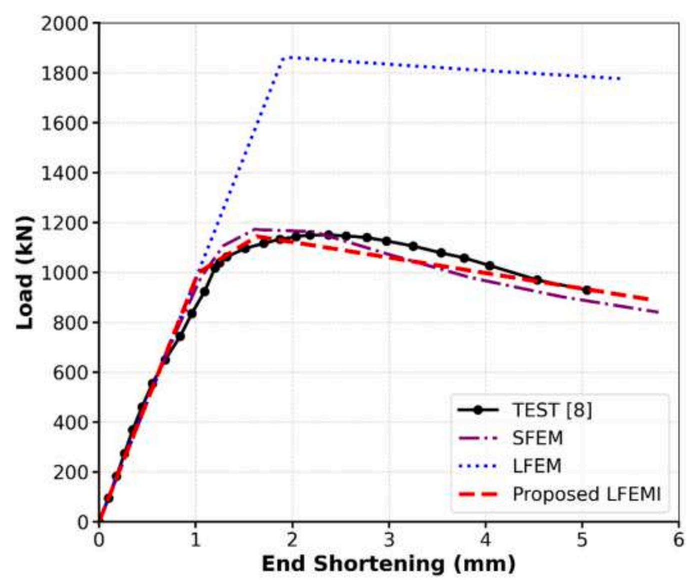

Fig. 15. Verification of load-end shortening curves SHS 150 × 150 × 4.

yield stress are 210 GPa, 0.3, and 500 MPa, respectively. The frame is subjected to two concentrated vertical loads, F, at the corners, and a lateral load of 0.0125 F, as shown in Fig. 12. As aforementioned, the frame is analyzed adopting SFEM, LFEM, and the LFEMI.

Results obtained from sophisticated SFEM with initial geometric imperfections are plotted in Fig. 13. The first Eigen buckling mode is scaled with a maximum amplitude of $B/400$, where B is the outside width of the SHS. Besides, the load-displacement curves resulting from the LFEM and LFEMI are depicted for comparison. It can be clearly seen that adopting the LFEM and implementing the material stress-strain relationship overestimates the failure load compared to the SFEM results. However, adopting the proposed stress-strain relationship within the LFEMI can predict the buckling behavior of steel frames comprising CFS box sections on a conservative side. In conclusion, Figs. (11) and (13) show the robustness and accuracy of the proposed approach in analyzing and designing CFS structures comprising box sections.

5.2. Comparisons between the proposed 1D line element method and experimental results

In this example, experimental results reported in Section 3 are further utilized to validate the proposed 1D line element approach for simulating columns with CFS box sections. Test results by Wang, et al. [8] which investigate the local buckling failure modes for such members, are plotted in Figs. 14 and 15. Two specimens (SHS 120 ×120×3 and 150 ×150×4) are modelled, while the material properties, loading configurations, and boundary conditions are adopted as reported in the test program. Load versus displacement curves for tested specimens are

Table 5
Ultimate loads for tested specimens made from CFS box sections.

specimens	Test[8]	SFEM		LFEMI		LFEM	
	P_u kN	P_u kN	Dif. %	P_u kN	Dif. %	P_u kN	Dif. %
SHS 120×120×3	835.46	830.50	-0.59%	828.69	-0.81%	1529.59	83.08%
SHS 150×150×4	1150.23	1140.5	-0.85%	1144.44	-0.50%	1862.23	61.90%

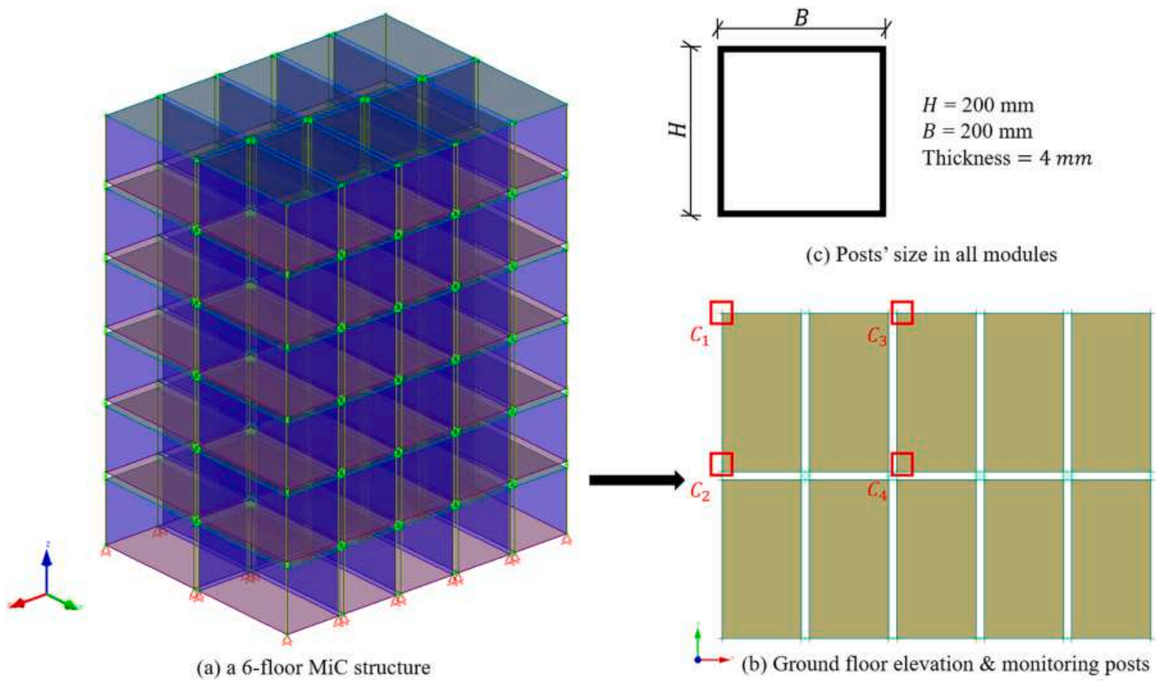

Fig. 16. A six-story MiC structure; geometric configurations and cross-section dimensions.

compared, as aforementioned, with different numerical approaches (i.e., SFEM, LFEM, and LFEMI). The numerical incorporation of the proposed compressive effective stress-strain relationship and the material tensile stress-strain relationship (Fig. 7) within the line FE method in ABAQUS represents the results from LFEMI and LFEM, respectively. Further, results from the more realistic but sophisticated SFEM are depicted for comparison.

Moreover, the ultimate loads for the tested specimens are summarized in Table 5, wherein the differences between the various numerical methods and experimental results are presented. From the results illustrated in Figs. 14 and 15 and Table 5, it can be clearly seen that the LFEMI considering the member local imperfections, can predict the load-displacement behavior of such members and in good agreement with test results and SFEM. Conversely, the LFEM utilizing the material tensile stress-strain curve overestimates the ultimate loads observed from load-displacement curves in Figs. 14 and 15.

5.3. A design example of the 1D line element for the design of MiC structures

A design example utilizing the proposed advanced design method is demonstrated here. A six-story MiC structure, depicted in Fig. 16, was investigated, where each module is designed with the dimensions of 3.2 m(height) x 3 m(width) x 6 m(length). The dead load (DL) and live load (LL) for floor slabs are taken as 4.0 kPa and 2.5kPa, respectively; while the dead load for module roof level is 0.9 kPa. The wind load (WL) is 2 kPa throughout the height. The critical design load combinations as following CoPHK [45] are considered, including 1.4DL+ 1.6LL, 1.4DL+ 1.4WL, and 1.2DL+ 1.2LL+ 1.2WL. The model is built using software NIDA [32], employing second-order nonlinear P-Δ-δ analysis to determine the internal forces and moments in the structural members. The relevant beam-column element allowing for member initial imperfection as well as the co-rotational framework for nonlinear analysis can be referred to the references [46,47]. Both global frame and local member imperfections are considered. The global frame imperfection is taken as H/200 while the member initial imperfection is taken as L/1000 as recommended in CoPHK [45], where H is building height and L is member length. Subsequently, the traditional effective width method (EWM) as outlined in ANSI/AISC 360–16 [9] is employed to estimate the cross-sectional capacity of the four columns labeled (C_1 − C_4), as shown in Fig. 16. Moreover, section capacity factors (SCF) were computed from two models: one utilizing the material stress curve (LFEM) and another incorporating the proposed effective stress-strain model (LFEMI) for comparison purposes.

The design results of four ground-floor columns were juxtaposed, comparing the application of the effective width method (i.e., AISC) with the advanced LFEM in NIDA, to showcase the efficiency and convenience of the proposed LFEMI. The modules are interconnected both vertically and horizontally through pin connections, as depicted in Fig. 16. The chosen column locations include building corners, the midpoints of both the long and short sides of the building and the center of the ground floor. These columns are constructed using cold-formed plates to form 200×200×4 sections, employing high-strength steel with $f_y = 690$ MPa, $E = 205$ GPa. The applied loads consist of a superimposed dead load of 4 kN/m^2 on the floor and a roof load of 0.9 kN/m^2. Additionally, live loads for both the floor and roof are set at 2.5 kN/m^2. In this investigation, the load combination of 1.4DL + 1.6LL is utilized.

Referring to Eq. (4) and Eq. (8), for the proposed model's posts, σ_p and σ_2 are computed to be 381 MPa and 265 MPa, respectively. Using the EWM, the sections' nominal axial and nominal flexural strengths are

Table 6
Section capacity factors for columns using different design methods.

Column Mark	AISC[1]	LFEM[2]	Diff.$^{2-1}$	LFEMI[3]	Diff.$^{3-1}$	SFEM[4]	Diff.$^{4-1}$
C1	0.729	0.427	-41%	0.772	6%	0.692	-5%
C2	0.590	0.342	-42%	0.619	5%	0.563	-4%
C3	0.687	0.400	-42%	0.725	5%	0.557	-6%
C4	0.587	0.328	-44%	0.594	1%	0.652	-5%

determined as 1030 kN and 89.577 kN.m, respectively. Then, the interactive equation, Eq. (10), is adopted for calculating the section capacity factor.

$$\frac{\overline{P}}{P_a}+\frac{\overline{M}_x}{M_{ax}}+\frac{\overline{M}_y}{M_{ay}}\leq 1.0 \tag{10}$$

where, $\overline{P}$ is the required compressive axial strength, $\overline{M}_x$ and $\overline{M}_y$ are required flexural strengths, P_a is the available axial strength and M_{ax} and M_{ay} are available flexural strengths. The section capacities of the selected columns employing different design methods are shown in Table 6.

From these findings, several conclusions can be made. Firstly, the LFEM, without accounting for the local buckling of the cold-formed sections, overestimates the column capacities by up to 40%. Conversely, utilizing the EWM and the proposed LFEMI yields safer designs by considering local buckling. The difference between the proposed LFEMI method and the EWM is around 5%, and it is noticeable that for posts controlled by compression instead of bending, the difference is only 1%. The LFEMI method not only streamlines the design process by enabling simultaneous design and analysis but also ensures a secure design without unnecessary conservatism. Theoretically, the SFEM method using shell element can provide more accurate results. However, this method need much modelling effort with significant increase of computer time.

6. Conclusions

Cold-formed steel structures show many benefits in construction such as cost-effectiveness, lightweight, high design flexibility and fast speed of construction. In this paper, an effective stress-strain model is proposed for integrated analysis and design of cold-formed steel structures with thin-walled sections. The presented material model, named the effective stress-strain relationship, was generated from the 2-dimensional (2D) shell finite element analysis (SFEA) of stub columns to include the member imperfections and cold-forming effect. Thus, the material nonlinearity could be captured from the proposed material model and is suitable for the direct analysis method for frame structures constructed from slender sections. The validation of the proposed material model included two stages. The first was conducted by comparing the results of frame analysis using shell finite elements and 1D line elements. In addition, the second stage of the validation compared the results obtained from LFEMI with experimental results. Based on the analyses results and comparisons presented in this paper, the following conclusion can be drawn.

- It was shown that frame analysis using the 1D line elements combined with the proposed effective stress-strain relationship and initial member imperfection (LFEMI) offered more conservative results than the sophisticated SFEA. This finding can be conjectured due to simpler and less computational efforts from the typical frame analysis approach using 1D line elements.
- The analysis method using LFEMI provided accurate results due to the inclusion of geometric imperfection and material nonlinearity. The load versus shortening curve obtained from LFEMI analysis matches well the test curves. Hence, the proposed effective stress-strain relationship can be recommended for advanced frame analysis, including the member imperfections for structures comprising members with slender sections.
- It was shown that the LFEMI is capable of facilitating both analysis and secure design. This approach finds applicability in various domains, including but not limited to full-scale structures, such as Modular Integrated Construction (MiC) systems. Notably, it holds promise for the advancement and proliferation of structural design involving the utilization of high-strength cold-formed steel sections.

Declaration of Competing Interest

The authors declare that they have no known competing financial interests or personal relationships that could have appeared to influence the work reported in this paper.

Acknowledgments

The first author is grateful for the research funding offered by Directorate of Research and Community Services of Universitas Tarumanagara, Indonesia. The second author is grateful for financial support from the competitive research projects - the research unit at Mansoura University for the project “Solar Energy Storage System Using a Medium of Sustainable Geopolymer Concrete” (MU-Eng-22–15).

References

[1] Yu C. Recent trends in cold-formed steel construction. Woodhead Publishing; 2016.
[2] Yu WW, LaBoube RA, Chen H. Cold-formed steel design. John Wiley & Sons; 2019.
[3] Afshan S, Rossi B, Gardner L. Strength enhancements in cold-formed structural sections-Part I: material testing. J Constr Steel Res 2013;vol. 83:177–88.
[4] Rossi B, Afshan S, Gardner L. Strength enhancements in cold-formed structural sections—Part II: Predictive models. J Constr Steel Res 2013;vol. 83:189–96.
[5] Gardner L, Yun X. Description of stress-strain curves for cold-formed steels. 2018/11/20/ Constr Build Mater 2018;vol. 189:527–38. 2018/11/20/.
[6] Ma JL, Chan TM, Young B. Material properties and residual stresses of cold-formed high strength steel hollow sections. J Constr Steel Res 2015;vol. 109:152–65.
[7] Somodi B, Kövesdi B. Residual stress measurements on cold-formed HSS hollow section columns. J Constr Steel Res 2017;vol. 128:706–20.
[8] Wang J, Afshan S, Schillo N, Theofanous M, Feldmann M, Gardner L. Material properties and compressive local buckling response of high strength steel square and rectangular hollow sections. Eng Struct 2017;vol. 130:297–315.
[9] AISC-360, *Specification for Structural Steel Buildings* (ANSI/AISC 360–16). Chicago: American Institute of Steel Construction, 2016.
[10] AISI, North American Specification for the design of cold-formed steel structural members. AISI S100–16. Washington D.C., USA: American Iron and Steel Institute, 2016.
[11] EC3, *Design of steel structures - Part 1.1: General rules and rules for buildings. BS EN 1993–1-1:2005+A1:2014*. Brussels, Belgium: European Committee for Standardization, 2014.
[12] Ma JL, Chan TM, Young B. Design of cold-formed high strength steel tubular beams. Eng Struct 2017;vol. 151:432–43.
[13] J.L. Ma, T.M. Chan, and B. Young, "Design of cold-formed high-strength steel tubular stub columns," Journal of Structural Engineering, vol. 144, no. 6, p. 04018063, 2018.
[14] B.W. Schafer, "Advances in the Direct Strength Method of cold-formed steel design," Thin-Walled Structures, vol. 140, pp. 533–541, 2019/07/01/ 2019.
[15] Lan X, Chen J, Chan TM, Young B. The continuous strength method for the design of high strength steel tubular sections in compression 2018;vol. 162:177–87.
[16] L. Gardner, X. Yun, and F. Walport, "The Continuous Strength Method – Review and outlook," Engineering Structures, vol. 275, p. 114924, 2023/01/15/ 2023.
[17] Du ZL, Liu YP, Chan SL. A second-order flexibility-based beam-column element with member imperfection. Eng Struct 2017;vol. 143:410–26.
[18] Chan SL, Liu YP, Liu SW. A new codified design theory of second-order direct analysis for steel and composite structures – from research to practice. Structures 2017;vol. 9:105–11.
[19] Gardner L, Yun X, Fieber A, Macorini L. Steel design by advanced analysis: material modeling and strain limits. Engineering 2019;vol. 5(2):243–9.

[20] Shanmugam NE, Chiew SP, Lee SL. Strength of thin-walled square steel box columns. J Struct Eng 1987;vol. 113(4):818–31.
[21] Chan SL, Kitipornchai S, Al-Bermani FGA. Elasto-plastic analysis of box-beam-columns including local buckling effects (pp) J Struct Eng 1991;vol. 117:1946–62.
[22] Pan W, Hon CK. Briefing: modular integrated construction for high-rise buildings. no 2020;vol. 173(2):64–8.
[23] Ferdous W, Bai Y, Ngo TD, Manalo A, Mendis P. New advancements, challenges and opportunities of multi-storey modular buildings – A state-of-the-art review. Eng Struct 2019;vol. 183:883–93. /03/15/ 2019.
[24] Thai HT, Ngo T, Uy B. A review on modular construction for high-rise buildings. Structures 2020;vol. 28:1265–90. /12/01/ 2020.
[25] Pan W, Yang Y, Pan M. Implementing modular integrated construction in high-rise high-density cities: perspectives in Hong Kong. Build Res Inf 2023;vol. 51(3): 354–68.
[26] H. K. C. website. Projects In Hong Kong. 2023. Available: ⟨https://mic.cic.hk/en/ProjectsInHongKong⟩.
[27] Abdelmageed S, Zayed T. A study of literature in modular integrated construction - Critical review and future directions. J Clean Prod 2020;vol. 277:124044.
[28] Lawson M, Ogden R, Goodier C. Design in modular construction. CRC Press; 2014.
[29] J. Murray-Parkes, Y. Bai, A. Styles, and A. Wang, "Handbook for the design of modular structures," *Monash University: Melbourne, Australia,* 2017.
[30] Lai Z, Varma AH. Effective stress-strain relationships for analysis of noncompact and slender filled composite (CFT) members. Eng Struct 2016;vol. 124:457–72.
[31] Du ZL, Liu YP, He JW, Chan SL. Direct analysis method for noncompact and slender concrete-filled steel tube members. Thin-Walled Struct 2019;vol. 135:173–84.
[32] N.I.D.A. User's Manual, Nonlinear Integrated Design and Analysis. NIDA 10 Online Documentation ⟨(⟩⟨http://www.nidacse.com⟩⟨)⟩. 2019.
[33] Abdelrahman AHA, Du ZL, Liu YP, Chan SL. Stability design of single angle member using effective stress-strain method. Structures 2019;vol. 20:298–308.
[34] Abaqus, "Analysis user's guide," 6.14–1 ed. Providence RI, USA: Dassault Systèmes Simulia Corp, 2014.
[35] Ma JL, Chan TM, Young B. Experimental investigation on stub-column behavior of cold-formed high-strength steel tubular sections. J Struct Eng 2016;vol. 142(5).
[36] Fang H, Chan TM, Young BJES. Structural performance of cold-formed high strength steel tubular columns 2018;vol. 177:473–88.
[37] J.L. Ma, T.M. Chan, and B. Young, "Cold-formed high-strength steel rectangular and square hollow sections under combined compression and bending," vol. 145, no. 12, p. 04019154, 2019.
[38] Yun X, Gardner L. The continuous strength method for the design of cold-formed steel non-slender tubular cross-sections. Eng Struct 2018;vol. 175:549–64.
[39] Dawson RG, Walker AC. Post-buckling of geometrically imperfect plates. *J Struct Div ASCE,* no 1972;98(1).
[40] Seif M, Schafer BW. "Local buckling of structural steel shapes," (pp) J Constr Steel Res 2010;vol. 66(10):1232–47.
[41] Huang Y, Young B. Structural performance of cold-formed lean duplex stainless steel columns. Thin-walled Struct 2014;vol. 83:59–69.
[42] W.L. Gao, A.H.A. Abdelrahman, S.W. Liu, and R.D. Ziemian, "Second-order dynamic time-history analysis of beam-columns with nonsymmetrical thin-walled steel sections," *Thin-Walled Structures,* vol. 160, p. 107367, 2021/03/01/ 2021.
[43] Chen L, Abdelrahman AHA, Liu SW, Ziemian Ronald D, Chan SL. "Gaussian Beam-Column Element Formulation for Large-Deflection Analysis of Steel Members with Open Sections Subjected to Torsion," (p) J Struct Eng 2021;vol. 147(12):04021206. 12/01 2021.
[44] Abdelrahman AHA, Liu SW, Liu YP, Chan SL. "Simulation of Thin-Walled Members with Arbitrary-Shaped Cross-Sections for Static and Dynamic Analyses," (p) Int J Struct Stab Dyn 2020;vol. 20(12):2050128.
[45] CoPHK, Code of Practice for the Structural Use of Steel 2011. 2011, Buildings Department Hong Kong SAR Government.
[46] Tang YQ, Ding YY, Liu YP, Chan SL, Du EF. Innovative displacement-based beam-column element with shear deformation and imperfection. Steel Compos Struct 2022;vol. 42(1):75.
[47] Tang YQ, Liu YP, Chan SL, Du EF. An innovative co-rotational pointwise equilibrating polynomial element based on Timoshenko beam theory for second-order analysis. Thin-Walled Struct 2019;vol. 141:15–27. 08/01/ 2019.